Experimental Analysis on Metal Friction Pairs for Symmetric Friction Connections

Hongliang Liu[a], Yuao Lin[b], LiangJiu Jia[c,*], Ping Xiang[d]

Tongji University, Shanghai, China

[a]hongliangliu@tongji.edu.cn; [b]2211319@tongji.edu.cn;
[c]lj_jia@tongji.edu.cn; [d]p.xiang@tongji.edu.cn

Abstract. The symmetric friction connection (SFC) is categorized as a slotted-bolt connection and is extensively used for dissipating seismic energy in earthquake-resistant structures. To investigate the effect of four types of metal friction pairs (Bisalloy450-Q460B, Bisalloy450-Q690E, Q690E-Q355B, and AISI 316L-Q355B) on the hysteretic performance of SFCs, one SFC was assembled for each type (four in total) for quasi-static testing. The test results indicate that the specimens with Bisalloy450-Q460B and Bisalloy450-Q690E friction pairs show excellent tribological and hysteretic performance. Under different bolt clamping forces, both exhibit high and stable friction coefficients of 0.79 and 0.59, respectively. In contrast, the specimens with AISI 316L-Q355B and Q690E-Q355B friction pairs exhibit fluctuating friction forces and friction coefficients, due to the poor tribological performance caused by the high mutual solid solubility of the metal friction pairs.

Keywords: Symmetric friction connection; Metal friction pair; Mutual solid solubility; Tribological performance; Hysteretic performance.

1 INTRODUCTION

The symmetric friction connection (SFC) is recognized as a crucial technology in designing low-damage structures. It can offer the benefits of maintaining a stable friction force and employing simple mechanical models, facilitating convenient analysis and design for structural vibration reduction. Extensive research has been conducted to explore the effects of interface conditions on the hysteretic performance of SFCs, such as interface pressure [1], material hardness [2], and loading rate [3]. Regarding friction materials, metals have been extensively used for friction pads, including brass [4], bronze alloy [5], and sprayed aluminum [6]. These friction materials exhibit varying differences in their static and kinetic friction coefficients, causing fluctuations in the friction force of SFCs during motion transitions. Even SFCs made of brass, known for their superior hysteretic performance, manifest some fluctuations in friction force within the same loading cycle [4]. Furthermore, these materials are expensive and not easily accessible. Consequently, this study endeavors to identify economically viable

B. Yuan et al. (eds.), *Proceedings of the 2024 8th International Conference on Civil Architecture and Structural Engineering (ICCASE 2024)*, Atlantis Highlights in Engineering 33,
https://doi.org/10.2991/978-94-6463-449-5_46

alternatives with stable hysteretic performance and elucidate potential reasons for the effects of different metal friction pairs on the hysteretic performance of SFCs.

2 MATERIALS AND METHODS

2.1 Design of SFC Specimens

As shown in Fig. 1(a), the SFC consists of a fixed plate, a slotted plate, two cap plates, two shims, some disc springs, eight countersunk bolts, and five M16 high-strength bolts. All SFC components underwent shot blasting before assembly to eliminate impurities adhered to metal surfaces. Fig. 1(b) shows the main geometric dimensions of the SFC. The maximum allowable displacement for each SFC was set at ±30 mm, comparable to the typical displacement capacity of conventional friction dampers.

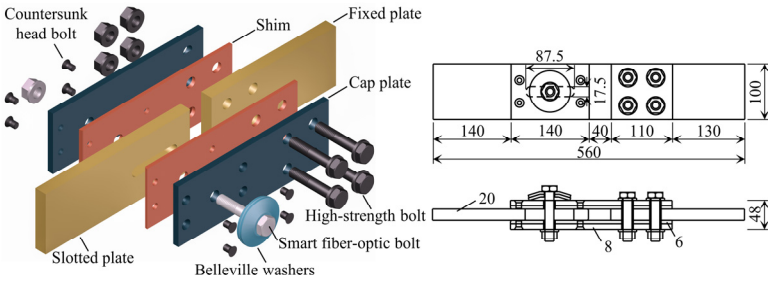

(a) Exploded view (b) Main geometric dimensions (unit: mm)

Fig. 1. Configuration of the SFC.

To investigate the effect of different metal friction pairs on hysteretic performance of SFCs, four types of friction pairs, namely, Bisalloy450-Q460B, Bisalloy450-Q690E, Q690E-Q355B, and AISI 316L-Q355B, were selected as the research objects. One SFC was assembled for each type of metal friction pair. Additionally, to study the effect of different bolt clamping forces on hysteretic performance of SFCs, three tests were conducted on the same SFC by applying different torques (T) to the smart fiber-optic bolt: 145 N.m, 190 N.m, and 240 N.m. Due to the high mutual solid solubility of the Q690E-Q355B friction pair, its friction force is difficult to predict. For safety reasons, a corresponding reduction in test torque was applied, namely, 95 N.m, 145 N.m, and 190 N.m. Different numbers of disc springs were configured for each test condition based on the applied torque to maintain the bolt clamping force. Characteristic parameters of the disc spring are presented in Table 1. The naming convention follows: B450Q460-T145 represents Bisalloy450 as the shim, Q460B as the slotted plate, and T145 as the test torque. The test plan is shown in Table 2.

Table 1. Properties of disc springs.

Inside Diameter (mm)	Outside Diameter (mm)	Thickness (mm)	Overall Height (mm)	Deflection (mm)	Load (kN)
17.1	55.8	4.8	6.2	1.4	68.5

Table 2. Summary of quasi-static tests.

Specimen	Series	T (N.m)	Disk springs configuration	Number of cycles
B450Q460	B450Q460-T145	145	1	25
	B450Q460-T190	190	2	20
	B450Q460-T240	240	3	30
B450Q690	B450Q690-T145	145	1	25
	B450Q690-T190	190	2	20
	B450Q690-T240	240	3	30
Q690Q355	Q690Q355-T95	95	1	25
	Q690Q355-T145	145	2	20
	Q690Q355-T190	190	2	30
316LQ355	316LQ355-T145	145	1	25
	316LQ355-T190	190	2	20
	316LQ355-T240	240	3	30

2.2 Quasi-static Testing of SFCs

The quasi-static tests were conducted using an MTS fatigue testing machine, with the loading device depicted in Fig. 2. The maximum load of the machine actuator is ±500 kN, and the maximum stroke is ±75 mm. All specimens were loaded under displacement control using a triangular wave with a loading rate of 3 mm/s. A smart fiber-optic bolt was used to monitor the bolt clamping force in real time.

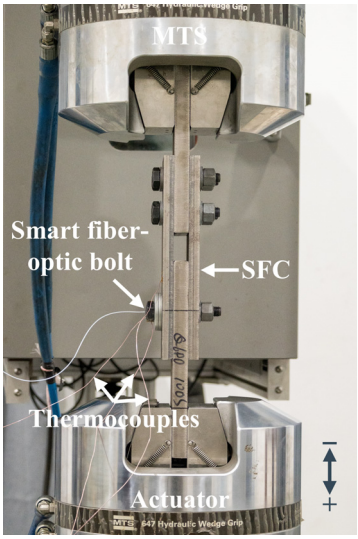

Fig. 2. Test setup of the SFC.

3 RESULTS AND DISCUSSION

3.1 Hysteretic Performance

Figure 3 shows the hysteresis curves under different test conditions. Influenced by compounds such as metal surface oxides and oil stains on contact surfaces, specimens B450Q460 and B450Q690 underwent a prolonged running-in stage during the first test, see Figs. 3(a) and (b). Their friction forces gradually increased with the number of cycles until they stabilized near a relatively high value. The sliding distances for specimens B450Q460 and B450Q690 when they entered the steady wear stage were 1080mm and 600mm, respectively. However, for specimens Q690Q355 and 316LQ355, their friction forces remained disordered throughout the first test and did not reach a stable state, as shown in Figs. 3(c) and (d). This is primarily because the metal friction pairs used in specimens Q690Q355 and 316LQ355 exhibit unstable tribological performance. In the second and third tests, all specimens rapidly entered the steady-wear stage. The ranking of hysteretic performance from best to worst is as follows: B450Q690, B450Q460, 316LQ355, and Q690Q355.

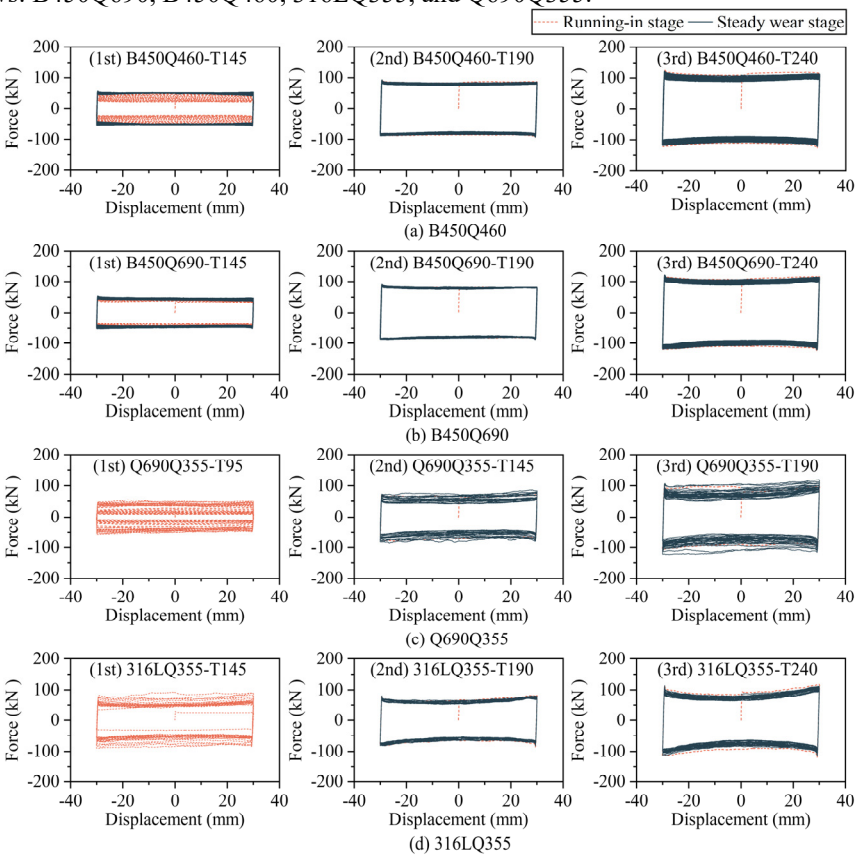

Fig. 3. Hysteresis curves under different test conditions.

3.2 Strength Degradation

As typical displacement-related energy dissipation devices, the SFC may encounter issues of friction force degradation as the number of cycles increases. Define f_i as the friction force of the ith cycle, which can be calculated by Eq. (1).

$$f_i = \frac{E_i}{D_i} \tag{1}$$

Where E_i is the work done by the friction force of the SFC in the ith cycle; D_i is the sliding distance of the ith cycle.

The friction force (f_i) is normalized with respect to the friction force of the first cycle of the test ($f_{initial}$). The variation in the dimensionless parameter ($f_i/f_{initial}$) with the number of loading cycles in different tests is depicted in Fig. 4. In the first test, specimens B450Q460 and B450Q690 quickly entered the steady wear stage. However, the friction forces of specimens Q690Q355 and 316LQ355 remained fluctuating throughout the first test. The maximum values of $f_i/f_{initial}$ for specimens B450Q460, B450Q690, Q690Q355, and 316LQ355 were 2.21, 1.38, 5.11, and 2.49, respectively. In the second test, the friction forces of specimens B450Q460, B450Q690, and 316LQ355 exhibited a stable degradation trend relative to the initial values, with the minimum values of $f_i/f_{initial}$ of 0.89, 0.95, and 0.86, respectively. The friction force of specimen Q690Q355 remained in a state of fluctuating degradation, with a minimum value of $f_i/f_{initial}$ of 0.66. In the third test, the degradation of the friction force was similar to that of the second test. The minimum values of $f_i/f_{initial}$ for specimens B450Q460, B450Q690, Q690Q355, and 316LQ355 were 0.8, 0.84, 0.65, and 0.76, respectively. The test results indicate that the order of hysteretic performance from best to worst is B450Q690, B450Q460, 316LQ355, and Q690Q355.

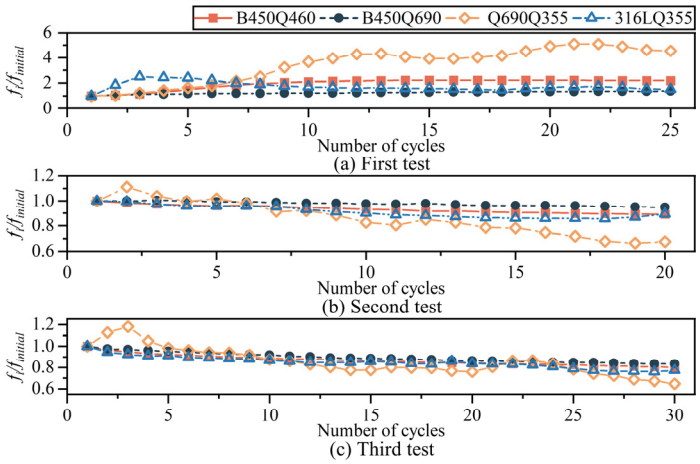

Fig. 4. Variation of the dimensionless parameter ($f_i/f_{initial}$) with the number of cycles.

3.3 Worn Surfaces

The worn surfaces of specimens B450Q460, B450Q690, Q690Q355, and 316LQ355 are depicted in Fig. 5. Specimens B450Q460 and B450Q690 exhibited uniform wear characteristics with relatively smooth worn surfaces, as shown in Figs. 5(a) and (b), respectively. However, as illustrated in Figs. 5(c) and (d), specimens Q690Q355 and 316LQ355 displayed numerous adhesion pits and grooves on the worn surfaces, indicating pronounced wear and poor tribological performance. An analysis by Rabinowicz [7] indicates a significant correlation between high mutual solid solubility and high wear and poor tribological properties. This further suggests that the high mutual solid solubility of Q690E-Q355B and AISI 316L-Q355B friction pairs is the reason for the unstable tribological and hysteretic performance of SFCs even under low bolt clamping forces.

(a) B450Q460 (b) B450Q690 (c) Q690Q355 (d) 316LQ355

Fig. 5. Worn surfaces.

3.4 Friction Coefficient

Variation in friction coefficient with total sliding distance for each specimen is illustrated in Fig. 6. As shown in Figs. 6(a) and (b), upon entering the steady wear stage, specimens B450Q460 and B450Q690 exhibited stable and predictable friction coefficients under different bolt clamping forces, with values of 0.79 and 0.59, respectively. As depicted in Fig. 6(c), the friction coefficient of specimen Q690Q355 remained fluctuating and unpredictable under different test conditions. In Fig. 6(d), specimen 316LQ355 demonstrated a relatively stable friction coefficient of 0.52 in the second and third tests. It can be concluded that after entering the steady wear stage, the tribological performance of specimens B450Q460 and B450Q690 is comparable and superior to that of specimen 316LQ355. Specimen Q690Q355 exhibits the poorest tribological performance.

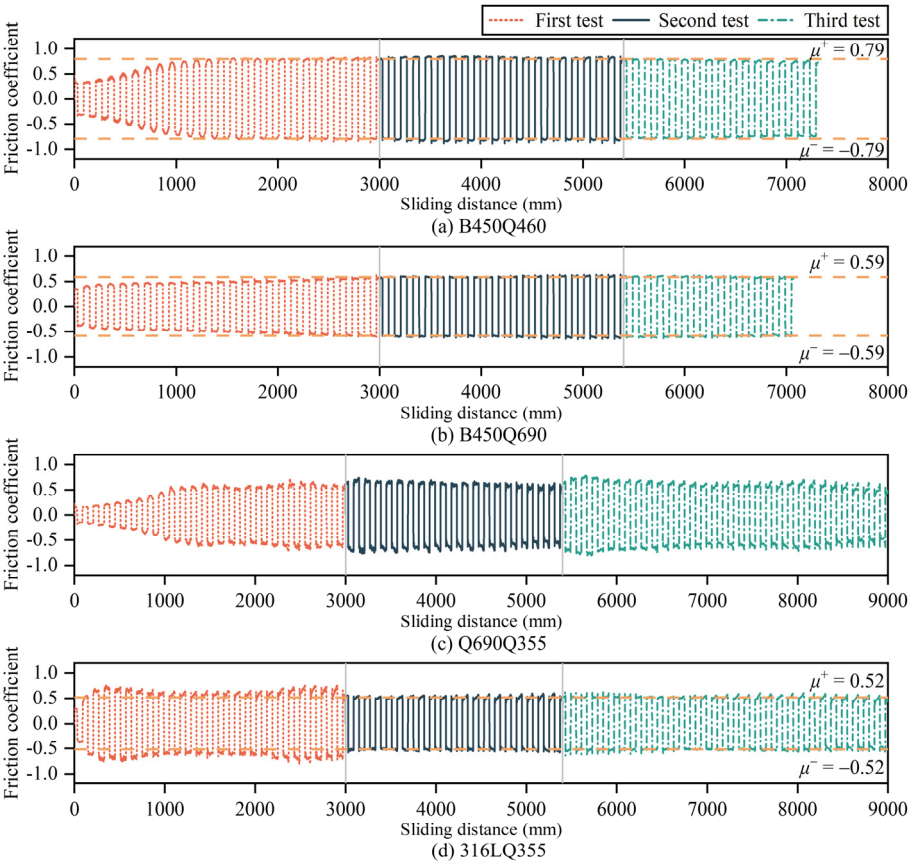

Fig. 6. Variation of the friction coefficient with the total sliding distance.

4 CONCLUSIONS

This paper describes the effect of metal friction pairs on the tribological and hysteretic performance of SFCs. The test results show that metal friction pairs with high mutual solid solubility tend to exhibit poor tribological performance, thereby resulting in unstable hysteretic performance of SFCs, as observed in the specimens with Q690E-Q355B and AISI 316L-Q355B friction pairs. The specimens with Bisalloy450-Q460B and Bisalloy450-Q690E friction pairs demonstrate stable tribological and hysteretic performance. The recommended friction coefficients for Bisalloy450-Q460B and Bisalloy450-Q690E friction pairs are 0.79 and 0.59, respectively. This study observed that different metal friction pairs all underwent a process transitioning from the running-in stage to the steady wear stage during the first test. In practical applications, it is recommended to preload the SFC before installation to advance the running-in stage, ensuring that the SFC can enter the steady wear stage with minimal sliding distance when anticipated earthquakes occur.

ACKNOWLEDGMENTS

The present work was carried out with financial support from the National Natural Science Foundation of China (Project Nos. 52178499, 51978529, and 52278525). The authors thank Prof. M. Li from Suzhou University of Science and Technology for providing the Dynamic Optical Sensing Interrogator and related guidance.

REFERENCES

1. Liu, H., Jia, L. J., Lin, Y. A., & Xiang, P. (2024). Effects of interface conditions on tribological and hysteretic behaviors of symmetric friction connections. Engineering Structures, 302, 117405. https://doi.org/10.1016/j.engstruct.2023.117405.
2. Golondrino, J. C. C., MacRae, G. A., Chase, J. G., Rodgers, G. W., & Clifton, G. C. (2020). Seismic behaviour of symmetric friction connections for steel buildings. Engineering Structures, 224, 111200. https://doi.org/10.1016/j.engstruct.2020.111200.
3. Loo, W. Y., Quenneville, P., & Chouw, N. (2014). A new type of symmetric slip-friction connector. Journal of Constructional Steel Research, 94: 11-22. https://doi.org/10.1016/j.jcsr.2013.11.005.
4. Grigorian, C. E., Yang, T. S., & Popov, E. P. (1993). Slotted bolted connection energy dissipators. Earthquake Spectra, 9(3): 491-504. https://doi.org/10.1193/1.1585726.
5. Morgen, B. G., & Kurama, Y. C. (2009). Characterization of two friction interfaces for use in seismic damper applications. Materials and Structures, 42: 35-49. https://doi:10.1617/s11527-008-9365-y.
6. Latour, M., Piluso, V., & Rizzano, G. (2014). Experimental analysis on friction materials for supplemental damping devices. Construction and Building Materials, 65: 159-176. https://doi.org/10.1016/j.conbuildmat.2014.04.092.
7. Rabinowicz, E. (1966). Compatibility criteria for sliding metals. In: Friction and Lubrication in Metal Processing. New York. pp. 90-102.